

Itinerancy-dependent non-collinear spin textures in SrFeO₃, CaFeO₃, and CaFeO₃/SrFeO₃ heterostructures probed via resonant x-ray scattering

Paul C. Rogge,¹ Robert J. Green,^{2,3} Ronny Sutarto,⁴ and Steven J. May¹

¹*Department of Materials Science and Engineering,
Drexel University, Philadelphia, Pennsylvania 19104, USA*

²*Department of Physics & Engineering Physics, University of Saskatchewan, Saskatoon, Saskatchewan S7N 5E2, Canada*

³*Stewart Blusson Quantum Matter Institute, University of British Columbia, Vancouver, British Columbia V6T 1Z4, Canada*

⁴*Canadian Light Source, Saskatoon, Saskatchewan S7N 2V3, Canada*

(Dated: June 25, 2019)

Non-collinear, multi- q spin textures can give rise to exotic, topologically protected spin structures such as skyrmions, but the reason for their formation over simple single- q structures is not well understood. While lattice frustration and the Dzyaloshinskii-Moriya interaction are known to produce non-collinear spin textures, the role of electron itinerancy in multi- q formation is much less studied. Here we investigated the non-collinear, helical spin structures in epitaxial films of the perovskite oxides SrFeO₃ and CaFeO₃ using magnetotransport and resonant soft x-ray magnetic diffraction. Metallic SrFeO₃ exhibits features in its magnetoresistance that are consistent with its recently proposed multi- q structure. Additionally, the magnetic Bragg peak of SrFeO₃ measured at the Fe L edge resonance energy asymmetrically broadens with decreasing temperature in its multi- q state. In contrast, insulating CaFeO₃ has a symmetric scattering peak with an intensity 10x weaker than SrFeO₃. Enhanced magnetic scattering at O K edge prepeak energies demonstrates the role of a negative charge transfer energy and the resulting oxygen ligand holes in the magnetic ordering of these ferrates. By measuring magnetic diffraction of CaFeO₃/SrFeO₃ superlattices with thick CaFeO₃ layers, we find that the CaFeO₃ helical ordering is coherent across 1 unit cell-thick SrFeO₃ layers but not 6 unit cell-thick layers. We conclude that insulating CaFeO₃ supports only a simple single- q helical structure in contrast to metallic SrFeO₃ that hosts multi- q structures. Our results provide important insight into the role of electron itinerancy in the formation of multi- q spin structures.

Introduction

Non-collinear spin textures provide a platform for the study of magnetic ordering and exchange interactions beyond conventional ferro and antiferromagnets, as well as have potential application in electronic devices and data storage [1, 2]. Of particular recent interest are materials that support multi- q non-collinear spin structures, where the spin structure is a superposition of multiple non-collinear orderings, denoted by ordering wavevectors, q , along different crystallographic directions, which can lead to topologically non-trivial spin textures, such as skyrmions [3–5]. Such multi- q states are known to arise from lattice distortions that result in a non-zero Dzyaloshinskii-Moriya (DM) interaction [6–8] or from frustration on triangular lattices [9, 10]. However, some materials have neither a DM interaction nor a frustrated lattice, yet still exhibit multi- q spin textures. These include elemental Nd [11], actinide monpnictides such as USb [12, 13], and, as very recently demonstrated, the cubic perovskite SrFeO₃ [14]. The underlying source of the multi- q behavior in these materials is unclear but is critical to understand in order to tune the properties of multi- q spin textures. Previous theoretical studies, however, point to a third consideration—electron itinerancy—such that coupling between itinerant and localized electrons leads to multi- q structures over single- q structures [15–20].

In order to investigate the role of itinerancy in multi- q spin structures, we synthesized epitaxial films of SrFeO₃ and CaFeO₃ and probed their magnetic structure using magnetotransport and resonant soft x-ray magnetic diffraction. While both materials exhibit incommensurate, non-collinear helical spin structures along $\langle 111 \rangle$ (see Fig. 1(a)) [21–28], SrFeO₃ is metallic whereas CaFeO₃ is insulating (CaFeO₃ exhibits an electronic phase transition ~ 170 K above its Néel temperature) [29, 30]. We demonstrate that the SrFeO₃ film exhibits the same complex magnetic phase diagram with distinct helical structures as measured in bulk samples, while further finding that transition temperatures between the magnetic phases more closely resembles Co-doped SrFeO₃, which we attribute to the moderate tensile strain induced by the substrate. Via resonant soft x-ray magnetic diffraction (RXMD), we show that the magnetic Bragg peaks of CaFeO₃ and SrFeO₃ exhibit significantly different behavior as a function of temperature. We discuss the SrFeO₃ results in context of the recently proposed multi- q structures [14], and from this we conclude that our results are consistent with insulating CaFeO₃ supporting a simple multi-domain, single- q structure. By synthesizing CaFeO₃/SrFeO₃ superlattices with different SrFeO₃ layer thicknesses, we find the CaFeO₃ helical structure is coherent through a single unit cell-thick SrFeO₃ layer but is not coherent when the SrFeO₃ layer is increased to 6 unit cells, even though both compounds support helical mag-

netic structures albeit with slightly different wavevector magnitudes. This result further suggests that the differences in the helical structures of SrFeO₃ and CaFeO₃ are more significant than a simple change to the magnitude of a single q wavevector. Our findings point to the importance of carrier itinerancy in multi- q spin structures and provide insight into the effect of heterostructuring dissimilar helical structures.

Film Results

Epitaxial, (001)-oriented SrFeO₃ and CaFeO₃ films were deposited by oxygen-assisted molecular beam epitaxy at ~ 650 °C with an oxygen partial pressure of 8×10^{-6} Torr (base pressure 4×10^{-10} Torr). The as-grown films were subsequently annealed in the deposition chamber by heating to ~ 600 °C in oxygen plasma (200 Watts, 1×10^{-5} Torr chamber pressure) and then cooled in oxygen plasma by progressively turning down the heater to zero output power over approximately one hour, followed by continued exposure to the plasma for another hour to ensure complete cooling to room temperature [31, 32]. Because ferrates are known to lose oxygen over time, prior to all measurements the films were re-annealed in oxygen plasma by the same post-growth process to mitigate oxygen deficiency.

SrFeO₃ was deposited on single crystal (La_{0.18}Sr_{0.82})(Al_{0.59}Ta_{0.41})O₃ (LSAT, +0.5% strain). CaFeO₃ was deposited on LaAlO₃ (+0.2% strain), as were superlattices of SrFeO₃/CaFeO₃. X-ray diffraction of the monolithic films is shown in Fig. 1(b). The simulated diffraction intensity of an ideal epitaxial film exhibits good agreement with measured data. Analysis of thickness fringes from x-ray reflectivity measurements shown in Fig. 1(c) indicate that the SrFeO₃ film is 14.2 nm thick (37 unit cells) and the CaFeO₃ film is 15.8 nm thick (42 pseudocubic unit cells), values that approximately match those obtained from the simulated diffraction data. Electrical transport, measured with Ag paint contacts in the van der Pauw geometry, further confirms the high-quality nature of the films. As seen in Fig. 1(d), CaFeO₃ exhibits a metal-insulator transition near 270 K, and both SrFeO₃ and CaFeO₃ have a 300 K resistivity comparable to bulk samples [29, 30]. The electrical transport confirms that CaFeO₃ is insulating below its Néel temperature, whereas SrFeO₃ is metallic.

The electrical transport and magnetoresistance of SrFeO₃ is known to exhibit rich features due to its helical magnetic ordering. Electrical transport, shown in Fig. 2(a), exhibits three anomalies as identified by the derivative of the resistivity with temperature (cooling). The first at 117 K is attributed to the onset of magnetic ordering, and a second and third anomaly occur at 110 K and 83 K, respectively. Additionally, the electrical resistivity exhibits hysteresis with temperature. These anoma-

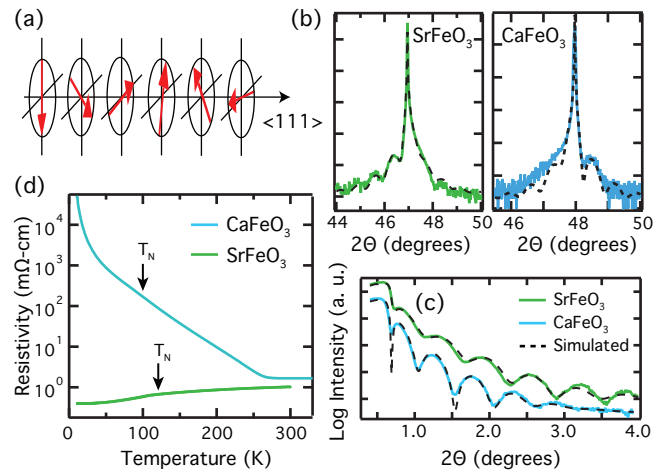


FIG. 1. (a) Schematic of the incommensurate, single- q helical magnetic ordering along one of the four equivalent $\langle 111 \rangle$ directions. Multi- q spin structures arise when the helical ordering exists along different $\langle 111 \rangle$ directions simultaneously. (b) Hard X-ray diffraction of a SrFeO₃ film deposited on LSAT(001) (0.5% tensile strain) and a CaFeO₃ film deposited on LaAlO₃(001) (0.2% tensile strain) measured at 300 K with $E = 8,047$ eV photons (Cu K_{α}). The simulated diffraction intensity of a perfect epitaxial film is shown by the dashed black line. (c) Hard X-ray reflectivity of the SrFeO₃ and CaFeO₃ films. Simulated intensity (dashed black lines) for a 14.2 nm thick (37 unit cells) SrFeO₃ film and a 15.8 nm thick (42 pseudocubic unit cells) CaFeO₃ film exhibits good agreement with measured. CaFeO₃ data are offset in y . (d) Electrical transport of the SrFeO₃ and CaFeO₃ films. Onset of helical ordering is denoted by the arrows (see text).

lies and hysteresis are consistent with previous measurements of bulk SrFeO₃, although a resistivity anomaly at the onset of helical ordering was not observed previously [25, 26, 33, 34]. We adopt the previously used nomenclature and label the regions as Phases I, II, and III [25], as shown in Fig. 2(a). No such anomalies are observed in the CaFeO₃ electrical transport [35].

Magnetoresistance [$MR = (\rho(H) - \rho(H=0))/\rho(H=0)$] measurements out to 9 T on SrFeO₃ are shown in Fig. 2(b) and further confirm the distinct nature of the three identified magnetic phases. The transition from a negative slope (e.g., between 155 K – 120 K) to a positive slope (e.g., 100 K) is consistent with the onset of helical ordering below 117 K [25]. At lower temperatures, the slope of the MR changes sign as the field increases, and a small degree of hysteresis is observed. This change in slope has been attributed to a transition to a field-induced fan- or cone-like helical state (Phases IV and V) [25]. Interestingly, this inflection point occurs at lower applied fields compared to previous measurements of both bulk and thin film samples of SrFeO₃, and instead is more comparable to Co-doped SrFeO₃ [26, 34].

In order to further distinguish Phase I and II, zero field cooling (ZFC) MR measurements were performed.

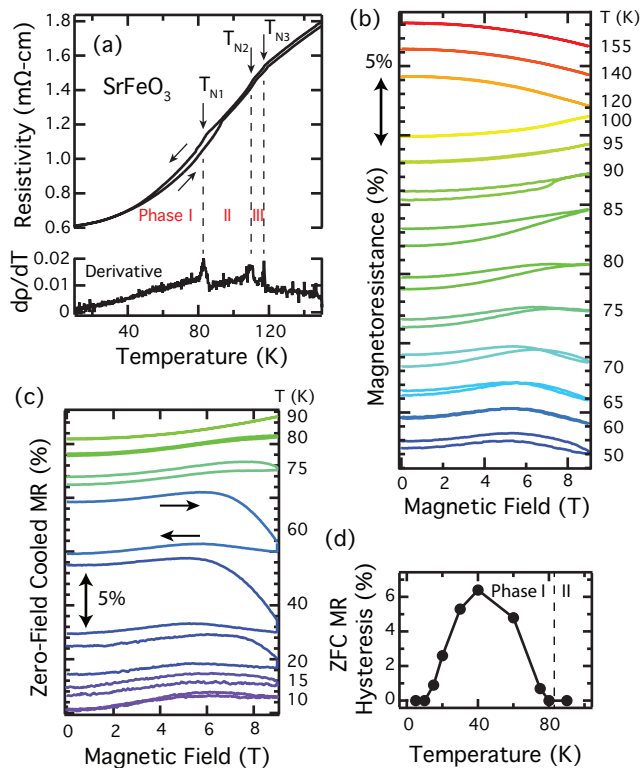


FIG. 2. (a) Electrical transport of the SrFeO₃ film exhibits three anomalies as indicated by the spikes in the derivative with temperature (lower panel) and are attributed to helical Phases I, II, and III. (b) Magnetoresistance measurements ($H \parallel [001]$, $I \parallel [100]$) of the SrFeO₃ film measured in succession with increasing temperature. The data are shifted in y for clarity. Double arrow scale bar denotes 5% MR. (c) Zero-field cooled (ZFC) MR measured at various temperatures. The data are shifted in y for clarity. (d) Percent hysteresis in the zero-field cooled MR as a function of temperature. The vertical, dashed line represents the transition between Phase I and II as identified by the electrical resistivity in (a).

After each measurement, the sample was heated to 150 K and then cooled with no applied field. The data are shown in Fig. 2(c) and reveal that the ZFC MR hysteresis is a strong function of temperature [hysteresis = $(\rho_{\text{ZFC}}(H=0) - \rho_{0T,9T,0T}(H=0)) / \rho_{\text{ZFC}}(H=0)$]. An onset of hysteresis is not observed until ~ 75 K that then increases with decreasing temperature. The ZFC MR hysteresis reaches a maximum near 40 K and vanishes below 20 K (see Fig. 2(d)). These results are consistent with previous work that attributed the ZFC MR hysteresis to H -induced domain rotation, where Phase I exhibits hysteresis but Phase II, notably, does not [25]. The onset of MR hysteresis here at ~ 75 K approximately correlates with the transition from Phase II to Phase I as identified by electrical transport (83 K) in Fig. 2(a). Additionally, the reduction in hysteresis at lower temperatures suggests that the critical field for domain rotation increases with decreasing temperature below 40 K and is consistent

with previous measurements that showed a critical field of ~ 15 T at 4.2 K [14, 25]. Similar MR measurements for CaFeO₃ were not possible due to its large resistivity below its Néel temperature (100 K). The main difference between these results and previous work is that the temperature range of Phase II is significantly smaller here (83 - 110 K) compared to bulk SrFeO₃ (56 - 110 K) [25] and previous measurements of a SrFeO₃ film (46 - 104 K) [26]. Instead, the Phase II temperature range of our SrFeO₃ film is comparable to Co-doped SrFeO₃, approximately equivalent to 1% Co-doping (SrFe_{0.99}Co_{0.01}O₃) in both bulk and thin-film samples [26, 34].

To gain further insight, we probed the magnetic ordering by measuring the resonant x-ray scattering at the Fe L edge along $q_H=K=L$ for the CaFeO₃ and SrFeO₃ films. Measurements were performed at the REIXS beamline at the Canadian Light Source. The (001)-oriented samples were mounted on a ~ 55 degree wedge in order to place the (111) planes in a symmetric scattering configuration. The scattered intensity measured as a function of temperature for the CaFeO₃ and SrFeO₃ films are shown in Figs. 3(a) and (b), respectively. Both films exhibit scattered intensity at values of q slightly suppressed compared to bulk samples: $q_{\text{CaFeO}_3} \sim 0.459 \text{ \AA}^{-1}$ (~ 1.37 nm helical wavelength) (1% suppressed; bulk: $q_{\text{CaFeO}_3} = 0.465 \text{ \AA}^{-1}$ [27, 28]); $q_{\text{SrFeO}_3} \sim 0.356 \text{ \AA}^{-1}$ (~ 1.76 nm helical wavelength) (3% suppressed; bulk: $q_{\text{SrFeO}_3} = 0.367 \text{ \AA}^{-1}$ [23]). The suppressed q vector for SrFeO₃ is again equivalent to approximately 1% Co-doping [34]. As seen in Fig. 3(a), the CaFeO₃ peak grows uniformly in intensity with decreasing temperature. Integrating the peak area and plotting as a function of temperature in Fig. 3(c) reveals an onset of magnetic ordering at ~ 100 K, which is slightly suppressed compared to bulk ($T_N = 120$ K [36]). Repeating for the SrFeO₃ film, we find an onset temperature of ~ 115 K, which correlates with $T_{N3} = 117$ K as determined from the electrical transport data, and is similarly suppressed compared to bulk ($T_{N3,\text{bulk}} = 133$ K [23]).

From the magnetic scattering data, the q vector as a function of temperature was extracted and is plotted in Fig. 3(d). Consistent with previous studies, the SrFeO₃ q vector increases in magnitude with decreasing temperature [23, 26], although here we additionally observe a small decrease below 80 K (Phase II \rightarrow I transition). In contrast, CaFeO₃ exhibits the opposite behavior, where the q vector decreases with decreasing temperature followed by a small increase at the lowest temperatures. Additionally, the overall change in q for CaFeO₃ is approximately 2x smaller than that exhibited by SrFeO₃.

Comparing the peak shape evolution with temperature between CaFeO₃ and SrFeO₃ in Figs. 3(a) and 3(b), respectively, reveals three striking contrasts. First, SrFeO₃ exhibits a significantly enhanced scattering intensity compared to CaFeO₃. As seen in Fig. 3(c), the scattered intensity for SrFeO₃ is over 10x greater

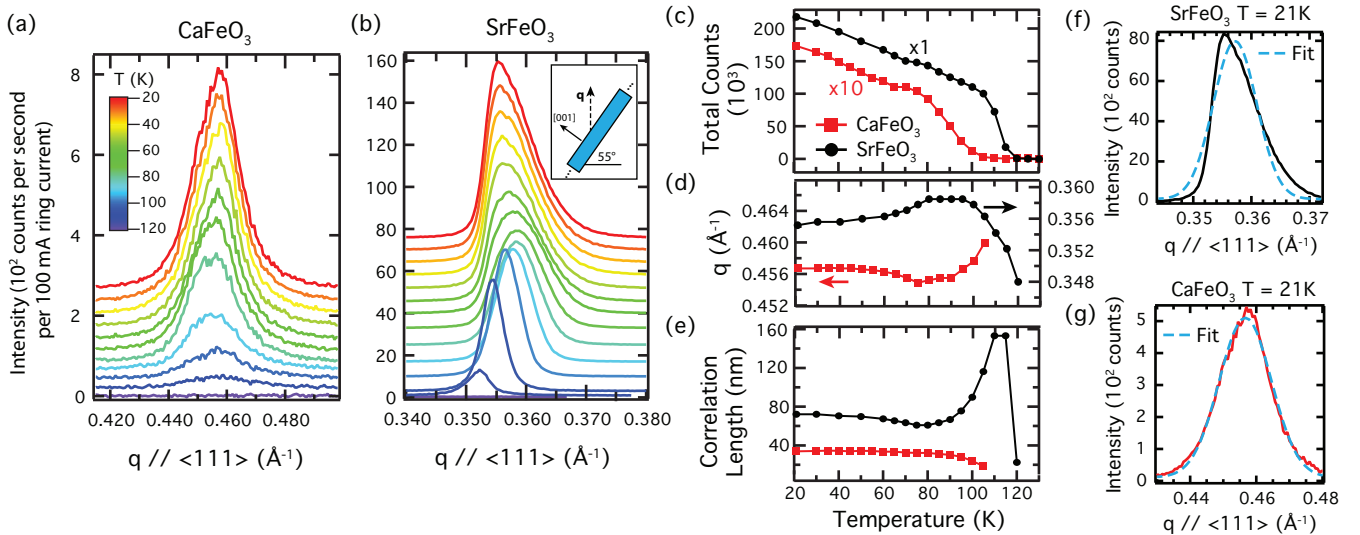


FIG. 3. (a) Resonant magnetic scattering along $q_{H=K=L}$ for the CaFeO_3 film ($E = 710.8$ eV) and (b) the SrFeO_3 film ($E = 710.6$ eV). Data are offset in y . Inset in (b) shows the scattering geometry. (c) Total scattered intensity for the CaFeO_3 and SrFeO_3 films. (d) Magnitude of the scattering vector and (e) correlation length derived from the FWHM of the scattering peak. The FWHM and value of q were determined by a Gaussian fit of the CaFeO_3 peaks; for SrFeO_3 the FWHM was manually extracted and q was determined by the maximum peak intensity. (f) Gaussian fit (dashed line) of the $T = 21$ K scattering peak (solid line) for SrFeO_3 and (g) CaFeO_3 .

than CaFeO_3 , which is unexpected given the same nominal film thickness, x-ray footprint, and detector settings (because the q vectors are different, the x-ray footprint for CaFeO_3 is reduced by $\sim 25\%$, which does not sufficiently explain the 10x reduction in intensity). The second observable difference between SrFeO_3 and CaFeO_3 is whereas the CaFeO_3 peak is initially broad and becomes more narrow with decreasing temperature, SrFeO_3 exhibits a narrow peak at the onset of helical ordering that then broadens with decreasing temperature. Converting the FWHM to a correlation length, $\xi = 2\pi/\text{FWHM}$, and plotting as a function of temperature in Fig. 3(e) demonstrates that the SrFeO_3 correlation length is initially 4x greater than CaFeO_3 and nearly 2x greater at lower temperatures. We note that the lower bound of the correlation length for an asymmetric Bragg peak of a thin film (e.g., the 111 reflection of a (001)-oriented film) is not limited to the film's thickness.

The third major contrast between SrFeO_3 and CaFeO_3 is the significantly different peak shape evolution exhibited by SrFeO_3 . With decreasing temperature, the peak asymmetrically broadens, where the expansion occurs at higher values of q , as highlighted in Fig. 3(f), where a symmetric Gaussian function cannot replicate the peak at 21 K. Such broadening was not observed in previous RXMD measurements of a SrFeO_3 film [26]. This broadening ceases below 80 K (see Fig. 3(e)), which correlates with the previously determined Phase II \rightarrow I transition in SrFeO_3 ($T_{N1} = 83$ K) extracted from electrical resistivity and ZFC MR measurements. In contrast, the CaFeO_3 scattering peak at 21 K is replicated by a sym-

metric Gaussian curve, as shown in Fig. 3(g).

Film results discussion

The helical spin structures of our SrFeO_3 film exhibit features equivalent to approximately 1% Co-doped SrFeO_3 [26, 34], as demonstrated by the narrowing of the Phase II temperature window, a decrease in the magnetic field strength at which the MR slope changes sign, a decrease in the magnitude of the q vector as probed by RXMD, and a decreased Néel temperature. A decrease in the q vector implies that the real-space length of the helix increases or, analogously, the helical angle between neighboring (111) planes, ϕ , decreases. A previous theoretical study of the helical state in these ferrates found that the helical ordering arises due to the double exchange effect coupled with a negative charge transfer energy, Δ [24, 37], where a negative Δ arises from the high formal oxidation state of Fe^{4+} in these ferrates [30, 31, 38, 39]. The helical angle tracks a single parameter $\delta = (\epsilon_F - \Delta + t_{pp})/(pd\sigma)$, where ϵ_F is the Fermi level position, t_{pp} is the oxygen-oxygen hopping amplitude, and $pd\sigma$ is the σ hybridization between p and d orbitals. Thus a decrease in ϕ corresponds to a decrease in δ , which can occur for an increased Δ , a decreased t_{pp} , and/or an increased $pd\sigma$. While tensile strain would be expected to decrease $pd\sigma$, it would also be expected to increase Δ and decrease t_{pp} , which can account for the reduction in δ and thus a reduction in q . In other words, we find that tensile strain acts to increase the ferromag-

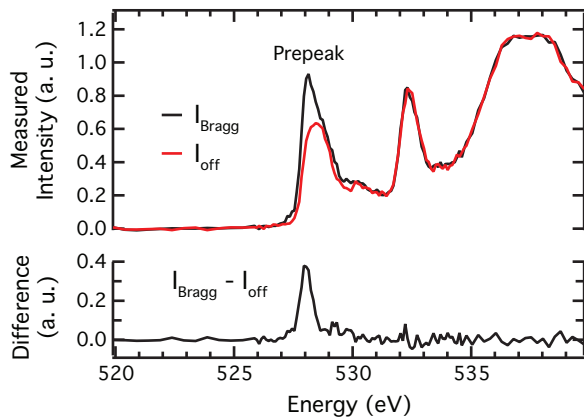


FIG. 4. (a) Intensity measured on the magnetic Bragg condition (I_{Bragg}) and off (I_{off}) across the O K edge for the SrFeO₃ film on LSAT at 21 K. The O prepeak is at 527.0-529.5 eV, and the peak at 531.5-533.5 eV is from the LSAT substrate. Lower panel shows the magnetic contribution to the scattering as determined by ($I_{\text{Bragg}} - I_{\text{off}}$).

netic contribution to the SrFeO₃ spin structure, likely due to an increase in Δ and/or a decrease in t_{pp} .

To demonstrate that a negative Δ plays an important role in the magnetic ordering in these ferrates, we measured the resonant magnetic scattering of the SrFeO₃ film as a function of energy across the O K edge on the Bragg condition ($q_z = 0.3548 \text{ \AA}^{-1}$) and slightly off the Bragg condition (detector offset by 2 degrees). As seen in Fig. 4, off the Bragg condition the measured intensity has features that resemble an x-ray absorption spectrum of these ferrates, as expected, where the strong prepeak feature between 527.0-529.5 eV arises from the oxygen ligand holes due to the negative charge transfer energy [31, 40, 41]. At the Bragg condition, there is a clear enhancement of the intensity within the prepeak region only. Taking the difference between the on and off Bragg conditions isolates the magnetic contribution to the scattered intensity and is shown in the lower panel of Fig. 4. The observation that the magnetic contribution to the scattered intensity occurs only in the prepeak region supports the conclusion that the charge transfer energy, Δ , is indeed negative and that the interaction between the O $2p$ and Fe $3d$ states is very strong. For completeness, the resonant magnetic scattering across the Fe L edge for the SrFeO₃ and CaFeO₃ films are shown in the Supplemental Material [35].

The resonant magnetic diffraction results for SrFeO₃ correlate with the magnetic phase transitions identified by electrical transport while highlighting distinct differences compared to CaFeO₃. The evolution of the SrFeO₃ scattering peak is notably unconventional; while the CaFeO₃ correlation length increases slightly upon cooling, as would be expected based on simple thermal considerations, the SrFeO₃ correlation length decreases

as a result of asymmetric peak expansion, which we attribute to the transition from Phase II to Phase I upon cooling. In contrast, the CaFeO₃ scattering peak remains symmetric down to at least 21 K and thus suggests that CaFeO₃ does not undergo additional magnetic phase transitions.

Recently, it has been proposed that SrFeO₃ supports multi- q magnetic structures [14] such that the spin structure is a superposition of multiple q vectors along different crystallographic directions. Specifically, Phase II is proposed to be a single-domain quadruple- q structure consisting of proper screw helical ordering with propagation vectors along the four $\langle 111 \rangle$ vectors of the cubic unit cell [14]. The lack of hysteresis in the ZFC MR in Phase II is consistent with a single-domain structure. Additionally, the much larger domain size (correlation length) in Phase II SrFeO₃ compared to CaFeO₃ could arise from a single-domain structure, although we cannot rule out that the CaFeO₃ film may be more defective than the SrFeO₃ film and thus has a smaller domain size.

The source of the asymmetric change in peak shape and decreased correlation length exhibited by SrFeO₃ at lower temperatures is harder to disentangle with these data alone. We discuss two possible scenarios. In the first scenario, a second, symmetric scattering peak forms at slightly higher q values, and grows in intensity with decreasing temperature. Such a scenario would be consistent with Ishiwata *et al.*'s [14] proposal of a multi-domain, double- q structure in Phase I, where each domain includes both a proper screw (q_1) and a vertical cycloid (q_2) ordering along one of the four $\langle 111 \rangle$ directions, where q_1 and q_2 are along different $\langle 111 \rangle$ directions, and the magnitude of q_1 is approximately equal to the magnitude of q_2 . In this picture, the two scattering peaks measured along the same $[111]$ direction arise from ordering in different domains: q_1 of proper screw along $[111]$ of one domain orientation and q_2 of vertical cycloid along $[111]$ of another domain orientation. An additional physical implication for this scenario is that the coherence length is dramatically underestimated because the two distinct peaks were treated as one broad peak. Ishiwata *et al.* also demonstrate that the scattering peak splits into 3 individual peaks upon transition to Phase I from Phase II, where the three peaks are given by (q, q, q') , (q, q', q) , (q', q, q) and $q' > q$. In a second possible scenario, the asymmetric peak broadening could be due to this splitting, where the precise peak shape depends on the experimental measurement conditions, in particular how q -space is scanned and the positions of the three peaks.

The main takeaway of both scenarios, however, is that the peak shape evolution of SrFeO₃ is not unexpected in context of the recent neutron diffraction measurements and is consistent with a transition from Phase II \rightarrow I. Thus our results, particularly the correlation length, highlight how x-ray scattering coupled with thin film effects pro-

vides another way to probe multi- q magnetic states beyond neutron diffraction measurements. Moreover, these results reveal that the Phase II \rightarrow I transition is not as abrupt as indicated in previous phase diagrams, because this transition has been determined based on electrical transport measurements. Here, electrical transport identifies Phase II within 110–83 K, but as seen by the change in the scattering peak shape (as proxied by the correlation length in Fig. 3(e)), the spin structure of SrFeO₃ evolves almost constantly with temperature from 110 to 85 K in Phase II. Thus the single domain Phase II state may be stable only within a very narrow temperature range just below T_{N2} (110 K). This may account for the lack of an observed decrease in total scattered intensity across the SrFeO₃ Phase II/I transition (single domain to multi-domain structure) because the still rapidly changing total intensity near 110 K could obscure this effect (see Fig. 3(c)).

These results provide important context for analyzing the CaFeO₃ scattering data. While previous studies have identified helical ordering in CaFeO₃ [27, 28], it is unknown if CaFeO₃ supports multi- q spin structures, which one may expect given its similarity to SrFeO₃. However, the data here demonstrate distinct differences between SrFeO₃ and CaFeO₃. The CaFeO₃ peak grows uniformly with decreasing temperature whereas the SrFeO₃ peak asymmetrically grows and exhibits larger changes in q . Additionally, the CaFeO₃ peak at low temperatures is symmetric, as seen in Fig. 3(g), suggesting that it does not replicate the presumed double- q ordering seen in SrFeO₃ at low temperatures. Although we cannot definitively determine the precise details of the spin structure within CaFeO₃, these results are consistent with a multi-domain, single- q helical structure, where different domains have helical ordering along one of the four $\langle 111 \rangle$ directions. A multi-domain helical state in CaFeO₃ is also consistent with the significantly reduced scattering intensity of CaFeO₃ compared to SrFeO₃—a 4x reduction would be expected given the 4 equivalent $\langle 111 \rangle$ directions.

A possible reason for SrFeO₃ hosting multi- q spin textures but not CaFeO₃ is their different itinerancies. Previous theoretical studies predict that single- q ordering can be destabilized in itinerant systems and instead multi- q structures are preferred [15, 17–19]. While a previous experimental study of the helimagnet Y₃Co₈Sn₄ has attributed itinerancy to the source of its multi- q state, it also has a DM interaction and lattice frustration that can result in multi- q structures [42]. Here, neither lattice frustration nor the DM interaction are present in cubic SrFeO₃, thus leaving electron itinerancy as the likely source of multi- q states in SrFeO₃. The fact that CaFeO₃ is insulating below its Néel temperature further supports the conclusion that it has a simple single- q spin structure. Future magnetic field-dependent neutron diffraction measurements could confirm a single- q structure in CaFeO₃. Interestingly, tuning the CaFeO₃

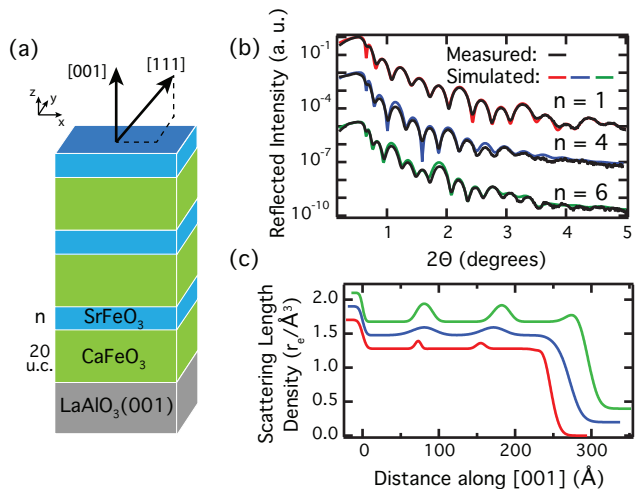


FIG. 5. (a) Schematic of the ferrate superlattices studied here. (b) X-ray reflectivity of three ferrate superlattices consisting of $[(\text{CaFeO}_3)_{20}/(\text{SrFeO}_3)_n] \times 3$ for $n = 1, 4,$ and 6 unit cells (u. c.) on $\text{LaAlO}_3(001)$ measured at 300 K with $E = 8,047$ eV photons ($\text{Cu } K_\alpha$; hard X-rays). Data for $n = 4$ and 6 are offset in y for clarity. (c) Real part of the scattering length density corresponding to the simulated reflectivity in (b); data are shifted by 0.2 and $0.4 r_e/\text{\AA}^3$ for the $n = 4, 6$ superlattices, respectively.

metal-insulator transition temperature (e.g., through A -site substitution ($\text{Ca}_{1-x}\text{Sr}_x\text{FeO}_3$ [43]) or modification of the atomic structure (i.e., octahedral rotations [44])) below its Néel temperature could enable further studies of the role of itinerancy in multi- q helimagnets.

Superlattice results and discussion

In order to probe how these different helical structures interact, we synthesized superlattices of CaFeO₃ and SrFeO₃. Superlattices consisting of $[(\text{CaFeO}_3)_{20}/(\text{SrFeO}_3)_n] \times 3$ for $n = 1, 4,$ and 6 unit cells were deposited on $\text{LaAlO}_3(001)$, as illustrated in Fig. 5(a). Non-resonant, hard X-ray reflectivity measurements, shown in Fig. 5(b), exhibit thickness oscillations and superlattice peaks consistent with the superlattices. The measured and simulated reflectivity for the $n = 1, 4,$ and 6 samples exhibits good agreement, and the corresponding scattering length density for the simulated data, shown in Fig. 5(c), confirms the superlattice structure. The top SrFeO₃ layer is obscured in the scattering length density for the $n = 1$ and 4 superlattices due to the surface roughness (10 Å and 14 Å, respectively). All three superlattices exhibit electrical transport similar to the monolithic CaFeO₃ film [35].

The resonant magnetic scattering data obtained from the three superlattices are shown in Fig. 6(a) and reveal three trends. First, as seen in Fig. 6(b), the onset temperature is near 115 K for all three superlattices.

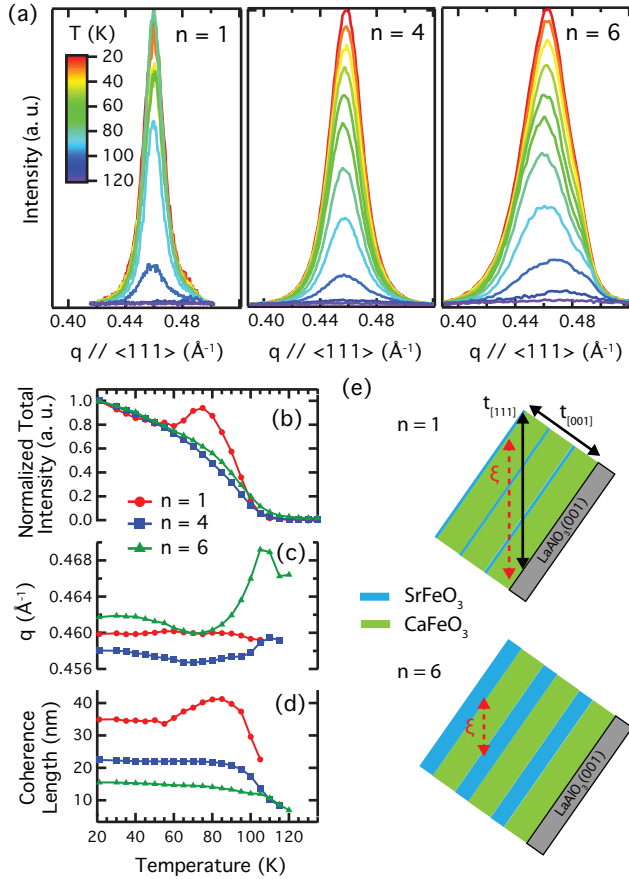


FIG. 6. (a) Resonant scattered intensity along $q_{H=K=L}$ for the three superlattices measured at different temperatures with $E = 711.0$ eV. The intensity at 21 K was normalized to unity because different detector settings were used among the superlattices. (b) Total scattered intensity, (c) q , and (d) correlation length as a function of temperature. (e) Schematic of the superlattice structure in the angled measurement geometry and depictions of the measured correlation length relative to the relevant film dimensions for the $n = 1$ and 6 superlattices.

This is 15 K higher than that measured for the monolithic CaFeO_3 film and is closer to that measured for the SrFeO_3 film ($T_{N3} = 117$ K). The intensity of the $n = 1$ superlattice trends differently with temperature compared to the other two superlattices, decreasing below 75 K and increasing again below 60 K. Second, the q vector of all three superlattices is approximately equal to that of the monolithic CaFeO_3 film and the trend of the temperature dependent q vector resembles that of the CaFeO_3 film as well.

Third, the correlation length decreases with increasing SrFeO_3 thickness, indicating that the SrFeO_3 layers disrupt the helical ordering. At the lowest temperatures, we find that the coherence length is 37 nm for the $n = 1$ superlattice and decreases to 16 nm for $n = 6$. For the $n = 1$ superlattice, the film thickness along $[111]$ is 41

nm, and in the simple case in which the magnetic domains are isotropic, this would indicate that the helical ordering is coherent through the entire superlattice such that the magnetic moments in the SrFeO_3 layers are ordered coherently with those in the neighboring CaFeO_3 layers. For $n = 6$, the 16 nm correlation length is comparable to the thickness of the individual CaFeO_3 layers (~ 13 nm), indicating that the helical ordering within the CaFeO_3 layers does not propagate through the now thicker SrFeO_3 layers. Although measuring down to $q = 0.35 \text{ \AA}^{-1}$, below the SrFeO_3 wavevector, did not show scattered intensity (not shown), the SrFeO_3 layers may be too thin to detect magnetic ordering, and thus we cannot ascertain definitively if the SrFeO_3 layers of the $n = 6$ superlattice are magnetically ordered or not. However, propagation through $n = 1$ but not $n = 6$ offers further evidence that the helical spin structures of SrFeO_3 and CaFeO_3 are different. Given that both compounds exhibit helical ordering with comparable wavevectors, it is surprising that only 6 SrFeO_3 unit cells disrupts the helical ordering if the spin texture is that of a single q helix. The coherence of the spin structure in the $n = 1$ superlattice implies that the multi- q spin texture of SrFeO_3 has been converted to a single- q texture due to proximity to CaFeO_3 and/or confinement effects.

In summary we have explored the role of electron itinerancy in the formation of non-collinear spin textures by studying the magnetic structures of metallic SrFeO_3 and insulating CaFeO_3 . We confirm that our SrFeO_3 film exhibits magnetotransport signatures consistent with its previously determined multi- q magnetic structure, and further demonstrate that its resonant soft x-ray magnetic diffraction behavior with temperature is consistent with a multi- q spin structure. CaFeO_3 , on the other hand, is found to exhibit significantly different magnetic diffraction characteristics compared to SrFeO_3 , which we attribute to a single- q spin helix in CaFeO_3 . Additionally, by synthesizing $\text{CaFeO}_3/\text{SrFeO}_3$ superlattices, we demonstrated that relatively thin layers (6 unit cells) of SrFeO_3 is sufficient to disrupt spin coherency through the superlattice, further supporting the conclusion that SrFeO_3 and CaFeO_3 have different helical magnetic structures. The lack of a Dzyaloshinskii-Moriya interaction and lattice frustration in cubic SrFeO_3 , and the presence of only a single- q helical ordering in insulating CaFeO_3 , supports the conclusion that electron itinerancy plays a critical role in the formation of the multi- q spin structures in SrFeO_3 . Thus, tuning electron itinerancy in other non-collinear spin structures can potentially be a path towards controlling multi- q spin structures and their topologically non-trivial spin structures.

We thank J. A. Borchers and M. R. Fitzsimmons for useful discussions. PCR and SJM were supported by the Army Research Office, grant number W911NF-15-1-0133, and film synthesis at Drexel utilized deposition instrumentation acquired through an Army Research Of-

fice DURIP grant (W911NF-14-1-0493). RJG was supported by the Natural Sciences and Engineering Research Council of Canada. Research described in this paper was performed at the Canadian Light Source, which is supported by the Canada Foundation for Innovation, Natural Sciences and Engineering Research Council of Canada, the University of Saskatchewan, the Government of Saskatchewan, Western Economic Diversification Canada, the National Research Council Canada, and the Canadian Institutes of Health Research.

-
- [1] A. Fert, N. Reyren, and V. Cros, “Magnetic skyrmions: Advances in physics and potential applications,” *Nat. Rev. Mater.* **2**, 17031 (2017).
- [2] F. Hellman, A. Hoffmann, Y. Tserkovnyak, G. S. D. Beach, E. E. Fullerton, C. Leighton, A. H. MacDonald, D. C. Ralph, D. A. Arena, H. A. Dürr, P. Fischer, J. Grollier, J. P. Heremans, T. Jungwirth, A. V. Kimel, B. Koopmans, I. N. Krivorotov, S. J. May, A. K. Petford-Long, J. M. Rondinelli, N. Samarth, I. K. Schuller, A. N. Slavin, M. D. Stiles, O. Tchernyshyov, A. Thiaville, and B. L. Zink, “Interface-induced phenomena in magnetism,” *Rev. Mod. Phys.* **89**, 025006 (2017).
- [3] U. K. Röbner, A. N. Bogdanov, and C. Pfleiderer, “Spontaneous skyrmion ground states in magnetic metals,” *Nature* **442**, 797–801 (2006).
- [4] S. Mühlbauer, B. Binz, F. Jonietz, C. Pfleiderer, A. Rosch, A. Neubauer, R. Georgii, and P. Böni, “Skyrmion lattice in a chiral magnet,” *Science* **323**, 915–919 (2009).
- [5] N. Nagaosa and Y. Tokura, “Topological properties and dynamics of magnetic skyrmions,” *Nat. Nano.* **8**, 899 (2013).
- [6] I. Dzyaloshinsky, “A thermodynamic theory of “weak” ferromagnetism of antiferromagnetics,” *J. Phys. Chem. Sol.* **4**, 241 – 255 (1958).
- [7] T. Moriya, “Anisotropic superexchange interaction and weak ferromagnetism,” *Phys. Rev.* **120**, 91–98 (1960).
- [8] P. Bak and M. H. Jensen, “Theory of helical magnetic structures and phase transitions in MnSi and FeGe,” *J. Phys. C Solid State Phys.* **13**, L881–L885 (1980).
- [9] T. Okubo, S. Chung, and H. Kawamura, “Multiple- q states and the skyrmion lattice of the triangular-lattice Heisenberg antiferromagnet under magnetic fields,” *Phys. Rev. Lett.* **108**, 017206 (2012).
- [10] C. D. Batista, S. Z. Lin, S. Hayami, and Y. Kamiya, “Frustration and chiral orderings in correlated electron systems,” *Rep. Prog. Phys.* **79**, 084504 (2016).
- [11] E. M. Forgan, E. P. Gibbons, K. A. McEwen, and D. Fort, “Observation of a quadruple- q magnetic structure in neodymium,” *Phys. Rev. Lett.* **62**, 470–473 (1989).
- [12] J. Rossat-Mignod, P. Burlet, S. Quezel, and O. Vogt, “Magnetic ordering in cerium and uranium monopnictides,” *Physica B+C* **102**, 237 – 248 (1980).
- [13] P. S. Normile, W. G. Stirling, D. Mannix, G. H. Lander, F. Wastin, J. Rebizant, F. Boudarot, P. Burlet, B. Lebech, and S. Coburn, “ $(U_{1-x}Pu_x)Sb$ solid solutions. I. magnetic configurations,” *Phys. Rev. B* **66**, 014405 (2002).
- [14] S. Ishiwata, T. Nakajima, J. H. Kim, D. S. Inosov, N. Kanazawa, J. S. White, J. L. Gavilano, R. Georgii, K. Seemann, G. Brandl, P. Manuel, D. D. Khalyavin, S. Seki, Y. Tokunaga, M. Kinoshita, Y. W. Long, Y. Kaneko, Y. Taguchi, T. Arima, B. Keimer, and Y. Tokura, “Emergent topological spin structures in a centrosymmetric cubic perovskite,” Preprint at <https://arxiv.org/abs/1806.02309> (2018).
- [15] I. Martin and C. D. Batista, “Itinerant electron-driven chiral magnetic ordering and spontaneous quantum hall effect in triangular lattice models,” *Phys. Rev. Lett.* **101**, 156402 (2008).
- [16] R. Ozawa, S. Hayami, K. Barros, G. W. Chern, Y. Motome, and C. D. Batista, “Vortex crystals with chiral stripes in itinerant magnets,” *J. Phys. Soc. Jpn.* **85**, 103703 (2016).
- [17] S. Hayami and Y. Motome, “Multiple- q instability by $(d - 2)$ -dimensional connections of Fermi surfaces,” *Phys. Rev. B* **90**, 060402(R) (2014).
- [18] S. Hayami, R. Ozawa, and Y. Motome, “Effective bilinear-biquadratic model for noncoplanar ordering in itinerant magnets,” *Phys. Rev. B* **95**, 224424 (2017).
- [19] S. Hayami, T. Misawa, Y. Yamaji, and Y. Motome, “Three-dimensional Dirac electrons on a cubic lattice with noncoplanar multiple- q order,” *Phys. Rev. B* **89**, 085124 (2014).
- [20] Y. Takehashi, D. Kojima, T. Otonari, and H. Miyagi, “Multiple helical spin density waves and magnetic skyrmions in itinerant electron system,” *J. Phys. Soc. Jpn.* **87**, 094712 (2018).
- [21] T. Takeda, Y. Yamaguchi, and H. Watanabe, “Magnetic structure of $SrFeO_3$,” *J. Phys. Soc. Jpn.* **33**, 967–969 (1972).
- [22] P. Adler, A. Lebon, V. Damjanović, C. Ulrich, C. Bernhard, A. V. Boris, A. Maljuk, C. T. Lin, and B. Keimer, “Magnetoresistance effects in $SrFeO_{3-\delta}$: Dependence on phase composition and relation to magnetic and charge order,” *Phys. Rev. B* **73**, 094451 (2006).
- [23] M. Reehuis, C. Ulrich, A. Maljuk, Ch. Niedermayer, B. Ouladdiaf, A. Hoser, T. Hofmann, and B. Keimer, “Neutron diffraction study of spin and charge ordering in $SrFeO_{3-\delta}$,” *Phys. Rev. B* **85**, 184109 (2012).
- [24] M. Mostovoy, “Helicoidal ordering in iron perovskites,” *Phys. Rev. Lett.* **94**, 137205 (2005).
- [25] S. Ishiwata, M. Tokunaga, Y. Kaneko, D. Okuyama, Y. Tokunaga, S. Wakimoto, K. Kakurai, T. Arima, Y. Taguchi, and Y. Tokura, “Versatile helimagnetic phases under magnetic fields in cubic perovskite $SrFeO_3$,” *Phys. Rev. B* **84**, 054427 (2011).
- [26] S. Chakraverty, T. Matsuda, H. Wadati, J. Okamoto, Y. Yamasaki, H. Nakao, Y. Murakami, S. Ishiwata, M. Kawasaki, Y. Taguchi, Y. Tokura, and H. Y. Hwang, “Multiple helimagnetic phases and topological hall effect in epitaxial thin films of pristine and Co-doped $SrFeO_3$,” *Phys. Rev. B* **88**, 220405(R) (2013).
- [27] P. M. Woodward, D. E. Cox, E. Moshopoulou, A. W. Sleight, and S. Morimoto, “Structural studies of charge disproportionation and magnetic order in $CaFeO_3$,” *Phys. Rev. B* **62**, 844–855 (2000).
- [28] S. Kawasaki, M. Takano, R. Kanno, T. Takeda, and A. Fujimori, “Phase transitions in Fe^{4+} ($3d^4$)-perovskite oxides dominated by oxygen-hole character,” *J. Phys. Soc. Jpn.* **67**, 1529–1532 (1998).

- [29] J. B. MacChesney, R. C. Sherwood, and J. F. Potter, “Electric and magnetic properties of the strontium ferrates,” *J. Chem. Phys.* **43**, 1907–1913 (1965).
- [30] J. Matsuno, T. Mizokawa, A. Fujimori, Y. Takeda, S. Kawasaki, and M. Takano, “Different routes to charge disproportionation in perovskite-type Fe oxides,” *Phys. Rev. B* **66**, 193103 (2002).
- [31] P. C. Rogge, R. U. Chandrasena, A. Cammarata, R. J. Green, P. Shafer, B. M. Lefler, A. Huon, A. Arab, E. Arenholz, H. N. Lee, T. L. Lee, S. Nemašák, J. M. Rondinelli, A. X. Gray, and S. J. May, “Electronic structure of negative charge transfer CaFeO_3 across the metal-insulator transition,” *Phys. Rev. Mater.* **2**, 015002 (2018).
- [32] P. C. Rogge, R. J. Green, P. Shafer, G. Fabbris, A. M. Barbour, B. M. Lefler, E. Arenholz, M. P. M. Dean, and S. J. May, “Inverted orbital polarization in strained correlated oxide films,” *Phys. Rev. B* **98**, 201115(R) (2018).
- [33] A. Lebon, P. Adler, C. Bernhard, A. V. Boris, A. V. Pimenov, A. Maljuk, C. T. Lin, C. Ulrich, and B. Keimer, “Magnetism, charge order, and giant magnetoresistance in $\text{SrFeO}_{3-\delta}$ single crystals,” *Phys. Rev. Lett.* **92**, 037202 (2004).
- [34] Y. W. Long, Y. Kaneko, S. Ishiwata, Y. Tokunaga, T. Matsuda, H. Wadati, Y. Tanaka, S. Shin, Y. Tokura, and Y. Taguchi, “Evolution of magnetic phases in single crystals of $\text{SrFe}_{1-x}\text{Co}_x\text{O}_3$ solid solution,” *Phys. Rev. B* **86**, 064436 (2012).
- [35] “See Supplemental Material at [URL] for the CaFeO_3 electrical transport and its derivative, resonant magnetic scattering of the SrFeO_3 and CaFeO_3 films across the Fe L edge, and the electrical resistance vs temperature of the three superlattice samples.”
- [36] F. Kanamaru, H. Miyamoto, Y. Mimura, M. Koizumi, M. Shimada, S. Kume, and S. Shin, “Synthesis of a new perovskite CaFeO_3 ,” *Mater. Res. Bull.* **5**, 257 – 261 (1970).
- [37] M. Azhar and M. Mostovoy, “Incommensurate spiral order from double-exchange interactions,” *Phys. Rev. Lett.* **118**, 027203 (2017).
- [38] T. Mizokawa, D. I. Khomskii, and G. A. Sawatzky, “Spin and charge ordering in self-doped Mott insulators,” *Phys. Rev. B* **61**, 11263–11266 (2000).
- [39] R. J. Green, M. W. Haverkort, and G. A. Sawatzky, “Bond disproportionation and dynamical charge fluctuations in the perovskite rare-earth nikelates,” *Phys. Rev. B* **94**, 195127 (2016).
- [40] M. Abbate, F. M. F. de Groot, J. C. Fuggle, A. Fujimori, O. Strebel, F. Lopez, M. Domke, G. Kaindl, G. A. Sawatzky, M. Takano, Y. Takeda, H. Eisaki, and S. Uchida, “Controlled-valence properties of $\text{La}_{1-x}\text{Sr}_x\text{FeO}_3$ and $\text{La}_{1-x}\text{Sr}_x\text{MnO}_3$ studied by soft-x-ray absorption spectroscopy,” *Phys. Rev. B* **46**, 4511–4519 (1992).
- [41] T. Tsuyama, T. Matsuda, S. Chakraverty, J. Okamoto, E. Ikenaga, A. Tanaka, T. Mizokawa, H. Y. Hwang, Y. Tokura, and H. Wadati, “X-ray spectroscopic study of BaFeO_3 thin films: An Fe^{4+} ferromagnetic insulator,” *Phys. Rev. B* **91**, 115101 (2015).
- [42] R. Takagi, J. S. White, S. Hayami, R. Arita, D. Honecker, H. M. Rønnow, Y. Tokura, and S. Seki, “Multiple-q non-collinear magnetism in an itinerant hexagonal magnet,” *Sci. Adv.* **4**, eaau3402 (2018).
- [43] T. Takeda, R. Kanno, Y. Kawamoto, M. Takano, S. Kawasaki, T. Kamiyama, and F. Izumi, “Metal-semiconductor transition, charge disproportionation, and low-temperature structure of $\text{Ca}_{1-x}\text{Sr}_x\text{FeO}_3$ synthesized under high-oxygen pressure,” *Solid State Sci.* **2**, 673 – 687 (2000).
- [44] A. Cammarata and J. M. Rondinelli, “Octahedral engineering of orbital polarizations in charge transfer oxides,” *Phys. Rev. B* **87**, 155135 (2013).